Eurographics Conference on Visualization (EuroVis) (2014)
N. Elmqvist, M. Hlawitschka, and J. Kennedy (Editors)

Bilateral Depth Filtering for Enhanced Vessel Reformation

Jan Kretchmer [1,2], Bernhard Preim[3] Marc Stamminger[1]

[1]Department of Computer Graphics,FAU Erlangen, Germany
[2]Siemens Healthcare Computed Tomography, Forchheim, Germany
[3]Department of Simulation and Graphics, Otto-von-Guericke University of Magdeburg, Germany

Abstract

Curved Planar Reformation is a powerful visualization technique for the diagnosis of vascular diseases. It allows an accurate centerline-driven investigation of vessel lumen while providing valuable anatomical context. Extended methods like Multipath Curved Planar Reformation, Centerline Reformation or Curved Surface Reformation provide additional flexibility by condensing entire vascular systems into rotatable views. Unfortunately, all these methods produce depth discontinuities because they operate in a projective fashion. While large discontinuities provide valuable hints about distinct anatomical contexts, small discontinuities, which frequently arise, have distracting effects on the visualization result and do not contribute significant information. In this paper we present a bilateral filtering technique which allows to selectively remove depth discontinuities without affecting discontinuities that carry information. The presented approach significantly improves the quality of vessel reformations, can be applied at interactive frame rates and is orthogonal to existing methods.

Categories and Subject Descriptors (according to ACM CCS): I.3.3 [Computer Graphics]: Picture/Image Generation—Display algorithms I.4.3 [Image Processing and Computer Vision]: Enhancement—Smoothing, Geometric correction

1. Background

Vascular visualization is an important tool in computer-aided diagnostics. For applications like stent-planning or the examination of calcifications and soft-plaques, an interactive display of vascular structures is of high importance. Since traditional slice-based viewing is not optimal to conduct the described tasks, a diverse range of visualization methods has been developed, ranging from dedicated transfer function designs for volume renderings [HST*03, LLY05] to surface-based methods [SOB*07, ZBG*07] and more abstract projection-based aproaches [BGP*11, MMV*13].

A well-established advanced visualization technique is Curved Planar Reformation (CPR) [KFW*02]. It is capable of generating rotatable 2D representations of entire vessel trees. By resampling medical datasets along rays derived from vessel centerlines, cut surfaces are generated, which allow a thorough inspection of patient-specific vasculature. The core feature of CPR visualizations is a simultaneous display of vessel lumen and anatomical context. This results in intuitive but yet highly diagnostic renderings of single vessels or entire vascular trees.

1.1. Vessel Reformation

The basic CPR algorithm [KFW*02] for visualizing a single vessel represented by a centerline works as follows: For a certain image plane (i.e. viewing direction) a scan line direction (i.e. x or y) is chosen. After this, scan lines parallel to the viewing plane are constructed to pass through the vessel centerline in world space. The scan lines describe a surface in 3D and are subsequently used to sample intensity values from the medical dataset. Eventually, the intensities are projected onto the image plane to visualize a centerline-driven curved cut through the dataset which can be rotated. The basic method was extended to the so-called Multipath CPR (mpCPR) [KFWG06]. It allows generating visualizations not only of a single vessel but of whole vascular trees which significantly increases contextual perception. To reduce occlusions, an untangled version of mpCPR (umpCPR) was later proposed by Kanitsar et al. [KWFG03].

A major problem with these approaches is that scan lines have to be as orthogonal to vessels as possible to produce a reasonable cross-sectional sampling. If vessel centerlines run parallel to the scan line direction, artifacts occur that may significantly reduce the visualized vessel lumen diame-

DOI: 10.2312/eurovisshort.20141150

ter. Mistelbauer et al. [MVB*12] propose Centerline Reformation (CR) which removes these scan line artifacts by propagating wave-fronts in the image plane. Even though their method operates in 2D image space, it is reported to have performance issues [AMB*13] and requires users to tweak thresholds. Recently, Curved Surface Reformation (CSR) was proposed [AMB*13]. CSR relies on a GPU-based rendering pipeline and resolves occlusions using depth buffer-inspired cost functions. The method does not suffer from the scan line-induced artifacts of CPR, mpCPR and umpCPR and is able to handle complex occlusion scenarios.

1.2. Depth Discontinuities in Vessel Reformation

A fundamental challenge when generating any type of multi-vessel reformation is the handling of occlusions that occur where different vessels get projected to the same region in image space. Current vessel reformation methods resolve visibility by associating influence zones in image space to certain (preferably the closest) vessels of the tree. This process effectively produces a depth map for a certain projection setup. mpCPR resolves visibility per pixel by choosing the vessel with the closest proximity in image space (in scan line direction); CR propagates distances in image space using a fast marching method and is thus not restricted to a certain scan direction; CSR employs more flexible cost functions that account for the distance of a vessel to the image plane and the distance to vessels in the projected image plane.

All these techniques have the common drawback of producing depth discontinuities in regions where influence zones change. Even current methods like CSR suffer from this problem. For switches from a very close region to a very far region these discontinuities serve the important purpose of illustrating a jump in context as mentioned in [AMB*13]. To emphasize this information, additional haloing techniques were proposed in [MVB*12]. When visualizing entire vascular trees with multiple branches, there are, however, many regions where different influence zones meet. In many constellations, the depth values of neighboring influence zones are not equal, but still very similar. In fact, often the depth values of zones are even close enough to generate cuts through the same anatomical structure which means they convey equivalent contextual information. In contrast to large depth discontinuities, these small jumps do not indicate contextual change. Unfortunately, even for Computed Tomography Angiography (CTA) runoffs with low-complexity vessel trees they lead to distracting artifacts like image discontinuities and scan line flickering.

Let us assume a CPR algorithm that is based on horizontal scan lines. In general, there are two types of discontinuities. (1) Horizontal artifacts occur at the end points of vessels. This is because once a vessel ends, the next scan line will be filled with image information derived from another vessel. (2) Vertical artifacts in contrast, occur when influence zones of projected neighboring vessels switch. Both types of artifacts are illustrated in Figure 1.

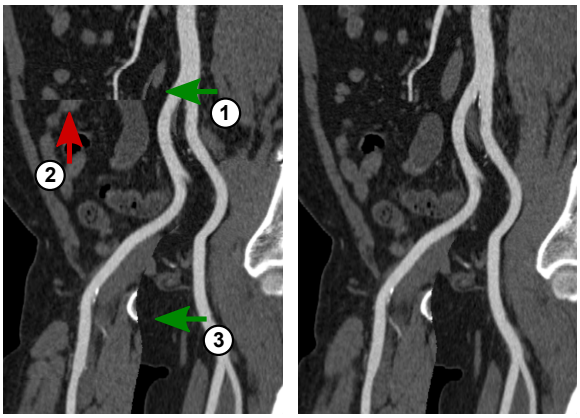

Figure 1: *Left:* Two types of artifacts typically occur in unfiltered CPR visualizations. Horizontal discontinuities (red) occur where vessels end. Vertical discontinuities (green) occur where influence zones of different vessels meet in scan lines. *Right:* Result of our bilateral depth filtering method. In this example, artifacts (1) and (2) originate from small depth discontinuities and were thus removed. The discontinuity (3) between the legs, in contrast, was preserved to keep indicating different anatomical contexts.

1.3. Bilateral Filtering

Bilateral filtering [TM98] is a powerful non-linear filtering concept which has become ubiquitous in image processing over the last two decades. The key concept is to extend a standard kernel-based filter by an additional modulation kernel and it is closely related to non-linear anisotropic diffusion [Bar02]. In the context of image filtering, this allows pixels to influence one another not only based on their spatial proximity but also based on the similarity of their pixel values. The filter applied in the image domain is commonly referred to as the *spatial filter* and the modulation filter that is based on the pixel values is commonly referred to as the *range filter*. The filtered image value $I_p{}'$ of a pixel at location p is computed by the following update rule

$$I_p{}' = \frac{\sum_{q\in\Omega} S(p-q)R(I_p-I_q)I_q}{\sum_{q\in\Omega} S(p-q)R(I_p-I_q)} \qquad (1)$$

where S and R represent the spatial kernel and the range kernel respectively and Ω represents the support of the filter.

Due to their adaptivity, bilateral filters have been extensively applied in the context of denoising depth maps [YK06, YYDN07] and surface meshes [FDCO03, LW05]. The key advantage over linear kernel-based filtering methods is that bilateral filters can avoid excessive smoothing at depth discontinuities. These discontinuities emerge for ex-

ample at edges of objects or between foreground and background regions. During bilateral filtering, regions in a depth map which expose similar depth values are usually set to influence each other more explicitly. Neighboring pixels with significantly differing depth values in contrast can be forced to have a reduced or virtually non-existing influence. This behavior allows to remove noise while preserving prominent discontinuities that might in fact be features.

2. Depth-Filtered Vessel Reformation

To improve the visual quality of CPR visualizations we make use of bilateral filtering. For this, we explicitly write the depth values to a 2D buffer which is then filtered. By successively applying the bilateral filter update rule (Equation 1) to all pixels p, the depth buffer gets smoother in each iteration. After the filtering process, the modified depth values can be used when sampling intensities from the original dataset.

During filtering, depth buffers are interpreted as discrete graphs with a 4-connected neighborhood. For the bilateral filter we chose the spatial filter S to be a discrete uniform Laplacian kernel and the range filter R to be a Gaussian-like kernel with zero means

$$S_w(x) = \begin{cases} w, & x = 1 \\ (1-w)|\Omega|, & x = 0 \end{cases} \qquad R_a(x) = e^{-x^2 a}. \qquad (2)$$

Both kernels have 1-ring support, which means x is either 1 or 0 and Ω only contains the direct neighbors of a pixel ($|\Omega| = 2$ for corner pixels, $|\Omega| = 3$ for border pixels and $|\Omega| = 4$ elsewhere). The user-adjustable relaxation parameter $w \in [0,1]$ controls the strength and $a \geq 0$ controls the anisotropy of the bilateral filter. The larger a is chosen, the less pixels influence each other across depth discontinuities.

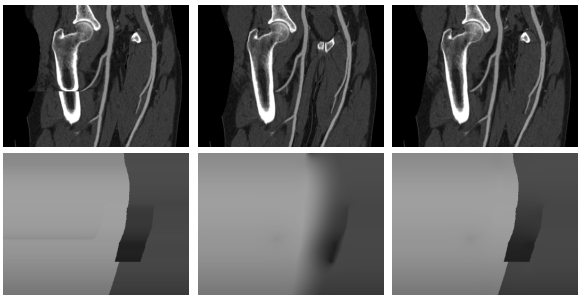

Figure 2: CPR visualizations (top row) and the corresponding depth maps (bottom row). *Left:* Depth discontinuity in the unfiltered CPR ($w = 0$) causes an artifact to appear in the femoral bone. *Center:* Isotropic linear filtering ($w = 1, a = 0$) removes this artifact but also smears out the intended discontinuity between the femoral arteries resulting in irritating patterns during CPR sampling. *Right:* Our bilateral filtering approach ($w = 1, a = 0.5$) removes the artifact in the femoral bone and preserves the discontinuity between legs.

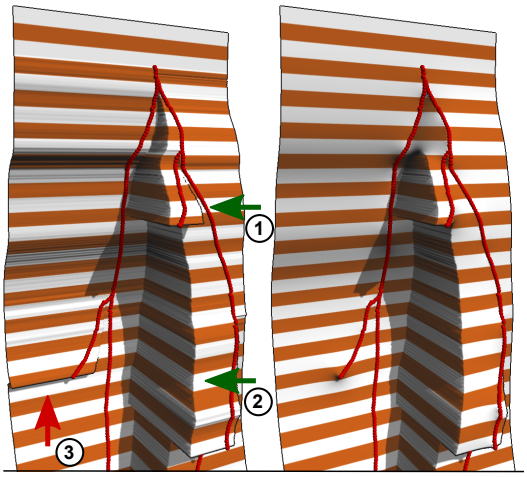

Figure 3: Geometric comparison of an unfiltered mpCPR (left) and a bilateral depth-filtered mpCPR (right). The scanning direction is illustrated by stripes. Vertical and horizontal artifacts are indicated by green and red arrows respectively. Small depth discontinuities (1 and 3) are removed during filtering while large ones (2) are preserved.

For $a = 0$ the filter behaves like an ordinary Laplacian kernel. Figure 2 shows close-ups of mpCPR visualizations of femoral vessels and the corresponding depth maps for different filtering setups.

To ensure that the filtered depth map still passes through the vessel centerlines, the corresponding pixels need to be constrained in depth. By flagging pixels close to centerlines as *fixed* and omitting them during smoothing iterations, they contribute to the 1-rings of their neighbors without being changed themselves. Filtering a depth map in this manner has a direct geometric interpretation related to Laplacian mesh fairing methods [SK01, Tau95]. The depth map can be viewed as a regular 3D surface mesh and the z component is being faired while some nodes are constrained. In contrast to linear Laplacian mesh fairing, however, the range kernel of the bilateral filter performs an implicit partitioning of the surface into regions of similar depth. Figure 3 shows a depth surface and its filtered counterpart where small depth discontinuities are removed while large discontinuities remain.

3. Performance and Implementation

To significantly improve the smoothness of a depth map, usually hundreds or even thousands of filter passes are necessary. This is because our mesh fairing-inspired filtering approach essentially means that we are solving a non-linear partial-differential equation using diffusion iterations [Bar02]. The required number of passes depends on the resolution of the depth map grid and on the desired target smoothness. For higher resolutions, more iterations are required so depth values can propagate properly across the

mesh. For example, for an mpCPR visualization with dimensions of 512×1024 pixels we typically choose 500 iterations. Each iteration requires over 0.5 million executions of the bilateral kernel in each pass (one per pixel). Even for a parallel CPU implementation this results in filtering times of several seconds, which prohibits interactive usage. To allow for interactive application of the filter, we prepared a GPU implementation that applies the filter in-place to all pixels in parallel. This results in acceptable filtering times which are in the same range as the CPR computation itself and which can be controlled by the number of iterations that is performed. See Table 1 for more detailed timings.

Table 1: Timings for mpCPR visualizations and 500 bilateral depth filter passes. Taken on an Intel Core i5 CPU with 4 cores @3.10GHz with 16GB RAM and an NVIDA GeFroce GTX 760 GPU. GPU timings include up- and downloading the depth buffers to and from GPU memory.

Resolution	mpCPR	Filter		Total
256×768	40 ms	CPU	2486 ms	2526 ms
		GPU	33 ms	74 ms
512×1024	113 ms	CPU	6748 ms	6862 ms
		GPU	75 ms	189 ms

4. Experimental Results

For many vascular visualization tasks, the major requirement is to represent the lumen of vessels as faithfully as possible. An important feature of our filtering approach is the ability to constrain depth maps in certain regions. By fixing the depth at centerlines as described in Section 2, the filtered depth map can be forced to exactly preserve the original cuts through vessels. If a centerline tree contains additional information about vessel diameters, the constrained regions can be extended to precisely include the whole lumen (similar concepts have also been proposed in the context of CPR generation itself [AMB*13,MVB*12]). This removes any effect of the filtering process on the visualization result inside the vessel lumen as demonstrated in Figure 4.

Since centerline regions are constrained, our filter has the most prominent impact in regions further away from vessels and leads to globally smoother cuts. A similar desirable effect was also produced in [AMB*13] using a hierarchical level of detail smoothing strategy. We point out that our method does *not* smooth any images themselves, it merely smoothes the depth pattern which is used when sampling the CPR image. As illustrated in Figure 5, an increased smoothness of depth maps in general leads to more natural cuts for CPRs. This effect is particularly prominent when no diameter information is available to preserve vessel lumen, or when vessels run roughly parallel to scan lines. In the unfiltered reformation in Figure 5, left, the discontinuity of the aortic arch significantly obscures the original vascular geometry. The depth-filtered reformation, in contrast, reveals

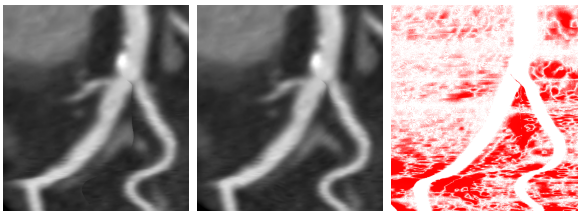

Figure 4: Vessel lumen comparison of a calcified coronary bifurcation. The depth-filtered mpCPR image (center) does not exhibit image discontinuity between vessels visible in the unfiltered mpCPR image (left). The difference image (right) shows that only the anatomical context is changed during filtering. The visualized vessel lumen is identical.

the true geometry and thus allows for more meaningful diagnostics. This is because the smoother cut surface adheres to the vessel geometry more faithfully.

5. Conclusion

In this article, we present a generic extension to vessel reformation that improves visual quality and contextual perception. Our key contribution is to introduce bilateral filtering as an intermediate step in the pipeline of CPR visualizations. Although inherent occlusion artifacts remain, the amount of depth map-related image artifacts in the final visualization can be significantly reduced with our method. The proposed approach can be used to improve virtually all existing CPR-like vessel visualization techniques, since they all suffer from depth discontinuities of some sort. We show that our method only impacts the visualization of anatomical context without side-effects onto the vessel lumen. Furthermore, we show that a GPU implementation allows a fast execution of the filter for interactive applications.

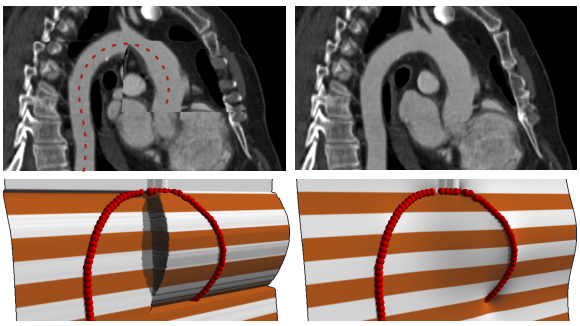

Figure 5: CPR visualization of an aortic arch (top) and corresponding depth surfaces (bottom). Due to the horizontal centerline trajectory at the top of the image, the unfiltered CPR (left) contains scan line-induced artifacts *inside* the vessel lumen. Since the filtered CPR is globally more smooth, this type of artifact is removed (right).

References

[AMB*13] AUZINGER T., MISTELBAUER G., BACLIJA I., SCHERNTHANER R., KÖCHL A., WIMMER M., GRÖLLER M. E., BRUCKNER S.: Vessel visualization using curved surface reformation. In *Proceedings of IEEE Visualization* (2013), vol. 19, pp. 2858–2867. 2, 4

[Bar02] BARASH D.: Fundamental relationship between bilateral filtering, adaptive smoothing, and the nonlinear diffusion equation. *IEEE Transactions on Pattern Analysis and Machine Intelligence 24*, 6 (2002), 844–847. 2, 3

[BGP*11] BORKIN M., GAJOS K., PETERS A., MITSOURAS D., MELCHIONNA S., RYBICKI F., FELDMAN C., PFISTER H.: Evaluation of artery visualizations for heart disease diagnosis. *IEEE Transactions on Visualization and Computer Graphics 17*, 12 (2011), 2479–2488. 1

[FDCO03] FLEISHMAN S., DRORI I., COHEN-OR D.: Bilateral mesh denoising. In *ACM Transactions on Graphics* (2003), vol. 22, ACM, pp. 950–953. 2

[HST*03] HIGUERA F. V., SAUBER N., TOMANDL B., NIMSKY C., GREINER G., HASTREITER P.: Enhanced 3d-visualization of intracranial aneurysms involving the skull base. In *MICCAI*. 2003, pp. 256–263. 1

[KFW*02] KANITSAR A., FLEISCHMANN D., WEGENKITTL R., FELKEL P., GROELLER E.: Cpr - curved planar reformation. In *Proceedings of IEEE Visualization* (2002), pp. 37–44. 1

[KFWG06] KANITSAR A., FLEISCHMANN D., WEGENKITTL R., GROELLER M.: Diagnostic relevant visualization of vascular structures. In *Scientific Visualization: The Visual Extraction of Knowledge from Data*, Bonneau G.-P., Ertl T., Nielson G., (Eds.), Mathematics and Visualization. 2006, pp. 207–228. 1

[KWFG03] KANITSAR A., WEGENKITTL R., FLEISCHMANN D., GROELLER M. E.: Advanced Curved Planar Reformation: Flattening of Vascular Structures. In *Proceedings of IEEE Visualization* (2003), pp. 43–50. 1

[LLY05] LUNDSTRÖM C., LJUNG P., YNNERMAN A.: Extending and simplifying transfer function design in medical volume rendering using local histograms. In *Eurographics Conference on Visualization (EuroVis)* (2005), pp. 263–270. 1

[LW05] LEE K.-W., WANG W.-P.: Feature-preserving mesh denoising via bilateral normal filtering. In *Computer Aided Design and Computer Graphics, 2005. Ninth International Conference on* (2005), IEEE, pp. 6–pp. 2

[MMV*13] MISTELBAUER G., MORAR A., VARCHOLA A., SCHERNTHANER R., BACLIJA I., KÖCHL A., KANITSAR A., BRUCKNER S., GRÖLLER M. E.: Vessel visualization using curvicircular feature aggregation. *Computer Graphics Forum 32*, 3 (June 2013), 231–240. 1

[MVB*12] MISTELBAUER G., VARCHOLA A., BOUZARI H., STARINSKY J., KÖCHL A., SCHERNTHANER R., FLEISCHMANN D., GRÖLLER M. E., SRÁMEK M.: Centerline reformations of complex vascular structures. In *IEEE PacificVis* (2012), pp. 233–240. 2, 4

[SK01] SCHNEIDER R., KOBBELT L.: Geometric fairing of irregular meshes for free-form surface design. *Computer aided geometric design 18*, 4 (2001), 359–379. 3

[SOB*07] SCHUMANN C., OELTZE S., BADE R., PREIM B., PEITGEN H.: Model-free surface visualization of vascular trees. In *EuroVis* (2007), pp. 283–290. 1

[Tau95] TAUBIN G.: A signal processing approach to fair surface design. In *SIGGRAPH* (1995), ACM, pp. 351–358. 3

[TM98] TOMASI C., MANDUCHI R.: Bilateral filtering for gray and color images. In *Sixth International Conference on Computer Vision* (1998), IEEE, pp. 839–846. 2

[YK06] YOON K.-J., KWEON I. S.: Adaptive support-weight approach for correspondence search. *IEEE Transactions on Pattern Analysis and Machine Intelligence 28*, 4 (2006), 650–656. 2

[YYDN07] YANG Q., YANG R., DAVIS J., NISTER D.: Spatial-depth super resolution for range images. In *IEEE Conference on Computer Vision and Pattern Recognition* (2007), pp. 1–8. 2

[ZBG*07] ZHANG Y., BAZILEVS Y., GOSWAMI S., BAJAJ C. L., HUGHES T. J.: Patient-specific vascular nurbs modeling for isogeometric analysis of blood flow. *Computer methods in applied mechanics and engineering 196*, 29 (2007), 2943–2959. 1